Annals of Botany **126**: 261–275, 2020
doi: 10.1093/aob/mcaa077, available online at www.academic.oup.com/aob

ANNALS OF BOTANY
Founded 1887

Processes controlling programmed cell death of root velamen radicum in an epiphytic orchid

Jia-Wei Li[1,2], Shi-Bao Zhang[3,*], Hui-Peng Xi[4], Corey J. A. Bradshaw[5] and Jiao-Lin Zhang[1,2,*]

[1]CAS Key Laboratory of Tropical Forest Ecology, Xishuangbanna Tropical Botanical Garden, Chinese Academy of Sciences, Mengla, Yunnan 666303, China; [2]Center of Plant Ecology, Core Botanical Gardens, Chinese Academy of Sciences, Mengla, Yunnan 666303, China; [3]Key Laboratory for Economic Plants and Biotechnology, Kunming Institute of Botany, Chinese Academy of Sciences, Kunming, Yunnan 650201, China; [4]Horticulture Department, Xishuangbanna Tropical Botanical Garden, Chinese Academy of Sciences, Mengla, Yunnan 666303, China; and [5]Global Ecology, College of Science and Engineering, Flinders University, GPO Box 2100, Adelaide, South Australia 5001, Australia
**For correspondence. E-mail sbzhang@mail.kib.ac.cn or zjl@xtbg.org.cn*

Received: 15 December 2019 Returned for revision: 24 January 2020 Editorial decision: 16 April 2020 Accepted: 18 April 2020
Electronically published: 22 April 2020

• **Background and Aims** Development of the velamen radicum on the outer surface of the root epidermis is an important characteristic for water uptake and retention in some plant families, particularly epiphytic orchids, for survival under water-limited environments. Velamen radicum cells derive from the primary root meristem; however, following this development, velamen radicum cells die by incompletely understood processes of programmed cell death (PCD).
• **Methods** We combined the use of transmission electron microscopy, X-ray micro-tomography and transcriptome methods to characterize the major anatomical and molecular changes that occur during the development and death of velamen radicum cells of *Cymbidium tracyanum*, a typical epiphytic orchid, to determine how PCD occurs.
• **Key Results** Typical changes of PCD in anatomy and gene expression were observed in the development of velamen radicum cells. During the initiation of PCD, we found that both cell and vacuole size increased, and several genes involved in brassinosteroid and ethylene pathways were upregulated. In the stage of secondary cell wall formation, significant anatomical changes included DNA degradation, cytoplasm thinning, organelle decrease, vacuole rupture and cell wall thickening. Changes were found in the expression of genes related to the biosynthesis of cellulose and lignin, which are instrumental in the formation of secondary cell walls, and are regulated by cytoskeleton-related factors and phenylalanine ammonia-lyase. In the final stage of PCD, cell autolysis was terminated from the outside to the inside of the velamen radicum. The regulation of genes related to autophagy, vacuolar processing enzyme, cysteine proteases and metacaspase was involved in the final execution of cell death and autolysis.
• **Conclusions** Our results showed that the development of the root velamen radicum in an epiphytic orchid was controlled by the process of PCD, which included initiation of PCD, followed by formation of the secondary cell wall, and execution of autolysis following cell death.

Key words: Epiphytic orchids, programmed cell death (PCD), root tip, velamen radicum, X-ray computerized tomography, transmission electron microscopy.

INTRODUCTION

The velamen radicum – a spongy tissue usually composed of multiple layers of dead cells on the outer surface of the epidermis of plant roots – is found throughout the monocotyledons, but is more common in epiphytic orchids (Pridgeon, 1987; Zotz *et al.*, 2017). It has been assumed to be an important adaptive characteristic of epiphytic orchids by providing a temporary but highly accessible reservoir of water for absorption (such as via precipitation or flow of canopy leachates) and the reduction of water loss (Benzing *et al.*, 1982; Pridgeon, 1987). The velamen radicum is also considered to support nutrient uptake (Zotz and Winkler, 2013), and provide an important protective role against UV-B radiation (Chomicki *et al.*, 2015). In addition, structures of the velamen radicum are highly diverse across different orchid genera, including variation in the number of cell layers as well as the absence or presence of thickening of the helical cell wall (Porembski and Barthlott, 1988). Velamen radicum structures are therefore useful traits to define relationships between various orchid taxa (Figueroa *et al.*, 2008; Aybeke, 2012; Pedroso-de-Moraes *et al.*, 2012). Despite these essential roles provided by the velamen radicum for epiphytic orchids and many studies focusing on its function, structure and comparative taxonomy, the developmental process of the velamen radicum remains poorly understood.

The cells of the velamen radicum develop from the primary root meristem, afterwards developing a secondary cell wall and, ultimately, obligate cell death occurs (Pridgeon, 1987). Although the maturation process of the velamen radicum has been identified as an example of developmental programmed

cell death (PCD), there is little understanding of how through changes in anatomy, and how at the molecular level the process is precipitated and regulated. Some forms of developmental PCD involve complete disappearance of the cell walls, which occurs *inter alia* in aerenchyma, endosperm and the mesophyll in senescent leaves and petals (Bozhkov *et al.*, 2005; Rogers, 2005, 2006; Gunawardena, 2008). In contrast, there are other examples where the cell walls are modified only slightly, even undergoing increased thickening, such as in vessels and fibres of the xylem (Escamez and Tuominen, 2014; Ruzicka *et al.*, 2015). Because both velamen radicum and xylem cells end up with thickened cell walls after going through developmental PCD, the process differs substantially from developmental PCD of aerenchyma or endosperm. We therefore hypothesize that the developmental process of the velamen radicum is similar to that observed in xylem vessels and fibres.

The process of developmental PCD in xylem vessels and fibres includes three, tightly linked phases: (1) the initiation phase; (2) the formation of the secondary cell wall; and, ultimately, (3) autolysis following cell death. During initiation, transcription factors belonging to NAC- (nascent polypeptide-associated complex) domain proteins act as major switches of xylem cell differentiation (Kubo *et al.*, 2005; Ko *et al.*, 2006; Zhong *et al.*, 2006; Ohashi-Ito *et al.*, 2010). Among them, vascular-related NAC-domain 6 (VND6) and VND7 are expressed preferentially in potential cells of vessels, thus governing their formation (Ohashi-Ito *et al.*, 2010). In contrast, secondary wall-associated NAC-domain protein 1 (SND1) is a principal regulator of fibre formation (Mitsuda *et al.*, 2005; Ko *et al.*, 2006). In addition, several hormones are involved in inducing the initiation phase of PCD in xylem, such as brassinosteroids (Yamamoto *et al.*, 1997; Du *et al.*, 2020) and ethylene (Pesquet and Tuominen, 2011).

Secondary cell wall formation in xylem is largely due to the biosynthesis of cellulose and lignin, and the biosynthesis of cellulose is tightly coupled with cytoskeleton-related factors (Oda *et al.*, 2005; Lacayo *et al.*, 2010; Carteni *et al.*, 2014). For example, cortical microtubules beneath the plasma membrane localize the cellulose synthase complexes which form the key enzyme of cellulose synthesis (Taylor *et al.*, 2000). For lignification, H_2O_2 is involved in peroxidase-mediated oxidative polymerization of cinnamyl alcohols to lignin (Novo-Uzal *et al.*, 2013). It has also been suggested that lignification is strongly reduced when gibberellin biosynthesis is inhibited, indicating that gibberellins are involved in activating the polymerization of lignin precursors (Tokunaga *et al.*, 2006).

During the final phase of autolysis, a typical plant PCD process is cytoplasmic degradation by autophagy, which includes formation of autophagosomes aiming at the vacuole (Bassham *et al.*, 2006; van Doorn and Papini, 2013). Vacuolar integrity plays a central role in autolysis in xylem vessels, because breakdown of the tonoplast can lead to leakage of hydrolytic enzymes from the vacuole, resulting in rapid degradation of organelles and nuclear DNA (Kuriyama, 1999; Obara *et al.*, 2001). Among the proteins regulating vacuole integrity, vacuolar processing enzyme (VPE) is particularly expressed during cell death (Hatsugai *et al.*, 2004; Rojo *et al.*, 2004; Nakaune *et al.*, 2005). In addition, various cysteine proteases such as xylem cysteine proteinase 1 (XCP1) and XCP2 have been implicated in the control of xylem PCD (Fukuda, 2000). Nucleases and RNases can also be responsible for the autolysis of xylem vessels (Ito and Fukuda, 2002).

Although the phases of maturation of both vessels and fibres are similar, there are some differences between these two tissues. For example, the differentiation of vessel elements occurs close to the cambium, but in fibres this differentiation occurs relatively far from the cambium (Courtois-Moreau *et al.*, 2009). In the velamen radicum, there have been no studies indicating the position of the developmental process in root tips. To quantify the process, we used the root tip of the epiphytic orchid *Cymbidium tracyanum*, whose large size allows spatial separation of the various developmental stages of the velamen radicum. We applied several novel tools to examine the major anatomical and molecular changes that occur during the developmental PCD of the velamen radicum, including a combination of transmission electron microscopy (TEM), X-ray micro-tomography, and transcriptome methods.

MATERIALS AND METHODS

Plant materials

We examined the developmental PCD of the velamen radicum in large-sized root tips of the epiphytic orchid *Cymbidium tracyanum*. This species grows on tree trunks in the sub-tropical forests of south-western China at altitudes ranging from 1200 to 2000 m above sea level. To minimize the potential effects of developmental differences among individuals of various ages on our experimental results, we selected 30 mature individuals of approximately uniform size. We planted these individuals in plastic pots containing a bark mixture in a greenhouse at Xishuangbanna Tropical Botanical Garden, southern Yunnan Province, China. The growing conditions were characterized by temperatures ranging from 25 to 33 °C, relative humidity between 60 and 90 %, and in 20 % full sunlight.

We defined the root 'tip' as the part of the root that extends from the physical end (tip) to the point where the colour of the velamen radicum changes to opaque white. To eliminate the effect of PCD in the root cap, we removed the distal 7 % of the total root tip, and then we divided the rest of the remaining root tip into three equal parts (i.e. proximal third, middle third and distal third). The thickness of the velamen radicum in the distal third was 150–350 µm, in the middle third it was 350–450 µ m, and in the proximal third it was approx. 450 µ m (Fig. 1).

Anatomy of the velamen radicum

We examined light microscopy images of transverse sections of the velamen radicum and photographed them using a digital camera mounted on a LeicaDM2500 microscope (Leica Microsystems Vertrieb GmbH, Wetzlar, Germany). We took the photographs at ×40 magnification to observe changes in cell size, the position of nuclei in the cells and the secondary cell wall of the velamen radicum.

For the observation from TEM, we excised pieces from a portion of the three sections of the velamen radicum in the root tip. Upon excision, we quickly infiltrated them in a 2.5

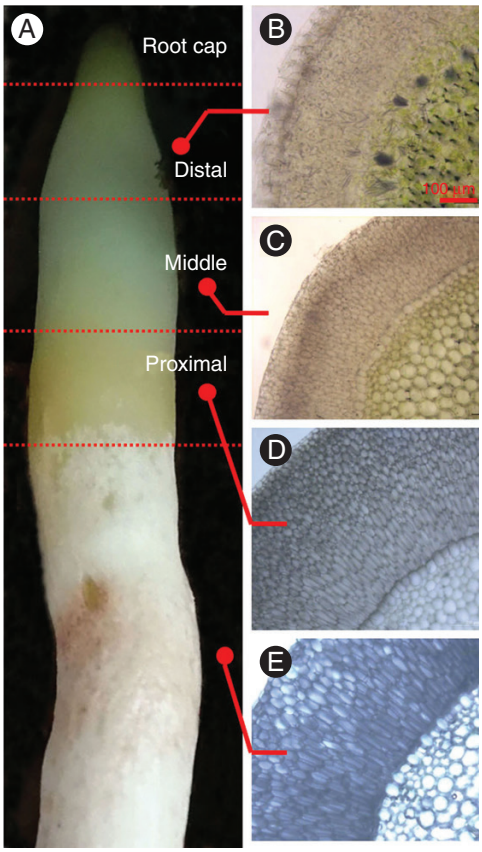

FIG. 1. Morphological and anatomical observations of the root tip from *Cymbidium tracyanum*. (A) Morphology of one root tip and three parts of the samples (distal third, middle third and proximal third); (B) cross-section of the velamen radicum from the distal third; (C) cross-section of the velamen radicum from the middle third; (D) cross-section of the velamen radicum from the proximal third; (e) cross-section of the velamen radicum from the mature part.

% glutaraldehyde fixative for at least 12 h, and then post-fixed them in 1 % osmic acid for 2 h before dehydrating them further in an ethanol and acetone series. After embedding the samples in LR white resin for 1 h, we obtained cross-sections using an ultramicrotome (Leica-R), staining each section afterwards with uranyl acetate and lead citrate. We viewed the ultrathin sections at magnifications of ×2000 to ×4000 using a JEOL JEM-1011 transmission electron microscope (JEOL Ltd, Tokyo, Japan) and then photographed the sections using an Olympus-SIS Mega view digital camera (Olympus Soft Imaging Solutions GmbH, Münster, Germany).

X-ray micro-computerized tomography scanning

We scanned six root tips (after cap removal) using X-ray micro-computerized tomography (Skyscan1275, Bruker, Belgium), with X-ray source settings of 50 kV and 200 µA. We recorded approx. 1000 images during each scan of around 30 min duration, across 180° comprising increments of 0.25°. We reconstructed the two-dimensional (2-D) tomographic projections into a single 3-D volume that we then split into approx. 1400 image slices using NRecon software. We analysed these reconstructed 2-D transverse images in Image J software to calculate the ratio of mature dead cells to living cells in the velamen radicum. We separated mature dead cells and living cells based on their differences in relative mass attenuation coefficients that we translated into an intensity value for each voxel.

Using Image J, we converted the reconstructed 2-D transverse images to a binary format to calculate the total area of the dead part of the velamen radicum. To detect the image showing the onset of maturity, we identified the first image where the voxel intensity value changed from one image to the next in the sequence. We named this first image '1' (meaning there were no dead areas visible in this image). To detect the first image showing full maturity of the velamen radicum, we identified the image where the total area of the dead section was no longer increasing. We named this image '10', with the total area of dead section defined as $area_{10}$. We divided this maturing section between image '1' and '10' into nine sections of equal length, and we obtained the eight images where each section in this region met (i.e. we named these eight images from '2' to '9', respectively), with the area of the dead section in each image defined as $area_2$, $area_3$… and $area_9$. We thus defined the 'mature' proportion as the $area_n$:$area_{10}$ ratio (where n = 1–9). Because each reconstructed 2-D transverse image had its reconstructed number which gradually increased from the proximal to the distal parts of the root tip, we were thus able to define the total length (l) of the root tip (except for the root cap) by calculating the total number (N) of images between the apex image after excising the root cap and the end image for development of the velamen radicum ($l = N_{apex} - N_{10}$). We defined the position of eight images by length (l_n) respectively, and calculated the total number of images between two images as $N_{apex} - N_n$, (where n = 1–9) (Fig. 2A). We were also able to calculate the proportional length (l) of the maturing section as the l_n:l ratio (where n = 1–9).

RNA sequencing, data processing and gene annotation

We peeled the velamen radicum of the three equal root tip parts (i.e. distal third, middle third and proximal third) with a knife. We extracted total RNA from each sample using the TIANGENRNA prep Pure kit (catalogue DP441, Beijing, China) according to the manufacturer's recommendations. We used a total of 1.5 µg of RNA per sample as input material for RNA-Seq library construction. We generated sequencing libraries using NEBNext Ultra RNA Library Prep Kitfor Illumina (NEB, USA) following the manufacturer's recommendations, to which we added index codes. We purified fragments of 250–300 bp in length with the AMPure XP system (Beckman Coulter, Beverly, USA), and assessed library quality on the Agilent Bioanalyzer 2100 system. After cluster generation, we sequenced the library preparations with an Illumina Hiseq 2000 platform, and obtained clean reads by removing reads containing poly-N strings and low-quality reads from the raw data, from which we calculated the Q20 and Q30 values, GC contents and sequence duplication of the cleaned data.

We undertook transcriptome assembly using the Trinity method (Grabherr *et al.*, 2011). We mapped clean reads back to the assembled transcriptome, and then obtained read

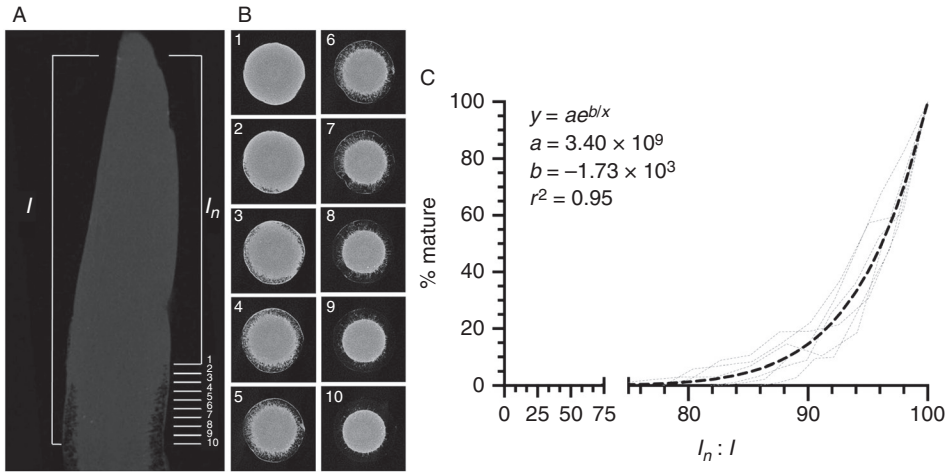

FIG. 2. Maturation process of the velamen radicum. (A) Reconstructed 2-D longitudinal section of the root tip from X-ray computerized tomography scans; (B) reconstructed 2-D transverse section of the velamen radicum of varying degrees of development from X-ray computerized tomography scans; (C) the mature proportion varies with l_n:l_{10}; the grey dashed lines show the change of six individuals, and the black dashed line shows the modified exponential model incorporating the mean value of all six individuals (with estimated coefficients a and b and their standard errors); r^2 = proportion of the variation as percentage maturity explained by the ratio l_n:l_{10}.

counts for each gene from the mapping results. We annotated gene function based on the following databases: Nr (NCBI non-redundant protein sequences), Nt (NCBI non-redundant nucleotide sequences), Pfam (Protein family), KOG/COG (Clusters of Orthologous Groups of proteins), Swiss-Prot (a manually annotated and reviewed protein sequence database), KO (KEGG Orthology database) and GO (Gene Ontology). We used KOBAS (Mao *et al.*, 2005) software to test the enrichment of differentially expressed genes (DEGs) in KEGG pathways.

Quantitative real-time PCR

To confirm the accuracy of the differentially expressed patterns observed in the transcriptome in this study, we randomly selected one gene that was upregulated in the middle third vs. the distal third, one that was downregulated in the middle third vs. the distal third, one that was upregulated in the proximal third vs. the distal third, one that was downregulated in the proximal third vs. the distal third, one that was upregulated in the proximal third vs. the middle third and one that was downregulated in the proximal third vs. the middle third (i.e. six genes in total) for quantitative real-time PCR (qRT-PCR) analysis.

We used the total RNA used from the transcriptome to synthesize single-stranded cDNAs for qRT-PCR analysis using the Prime-Script™ RT Reagent Kit with gDNA Eraser (TaKaRa, Dalian, China). We undertook qRT-PCR analysis using SYBR Premix Ex Taq™ II (TaKaRa, Dalian, China) on a CFX96 Touch Real-Time PCR System (Bio-Rad, California, USA) according to the manufacturer's protocol. We used the actin gene as an internal reference for calculating relative expression with the $2^{-\Delta\Delta ct}$ method. We analysed each sample in triple biological and technical replicates. The specific primers used for qRT-PCR analysis are listed in Supplementary data Table S1.

Statistical analysis

We undertook a differentially expressed analysis of two positions with three biological replicates using the DESeq package (1.10.1) in R (Love *et al.*, 2014), and determined the DEGs in the digital gene expression data by using a model based on the negative binomial distribution. We adjusted the resulting Type I error probabilities (P) using the Benjamini and Hochberg's approach to correct for the false discovery rate. We assigned genes with an adjusted $P_{adj} < 0.05$ found by DESeq as differentially expressed.

RESULTS

Anatomical traits of the velamen radicum

Using light microscopy, we observed changes in cell shape, the position of nuclei and the formation of secondary, wall-like striations during the process of cell death. During early differentiation of the distal third of the velamen radicum, the cells were small and spherical, with the nuclei in the centre of the cell. As development progressed in the middle third, the cells of the velamen radicum increased in size, with their nuclei pressed against the cell wall by pressure from the large vacuole. At the final stage of development in the proximal third, the cell walls of the velamen radicum were thickened by long strands of cellulose and lignin that formed a mesh-like appearance (Fig. 3A).

According to TEM, during early differentiation, the cells in the distal third had dense cytoplasm with a high density of various organelles and several small vacuoles. At this stage, the appearances of the nuclei, mitochondria and ribosomes were normal. In the middle third, with increasing vacuole size, the cytoplasm seems to decrease and the nuclei are pushed against the cell wall. With the deposition of secondary cell wall material in the proximal third, the nucleus became rounder in shape, suggesting that the vacuole was providing less pressure following vacuolar rupture. Secondary images from the proximal

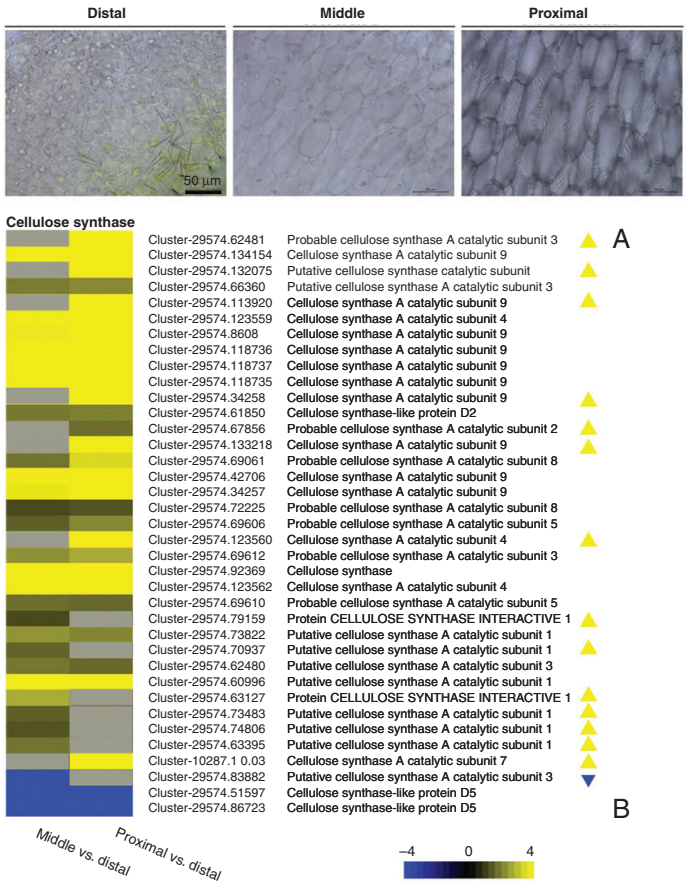

FIG. 3. Changes in expression of transcripts involved in cellulose synthesis and anatomy of cell walls. (A) Light microscopy images of velamen radicum cells from three parts of the root tip (i.e. the distal third, middle third and proximal third); (B) expression heat maps for cellulose synthase detected through differentially expressed gene analysis. Yellow or blue represents upregulation or downregulation, grey with yellow or blue arrowheads indicates that the genes were upregulated or downregulated, but the P_{adj} was ≥0.05. The scale bar represents the $\log_2$ fold change in differentially expressed genes.

third show a cell of the velamen radicum at the last stage of maturation with final autolysis of all cell contents (Fig. 4C).

According to the X-ray micro-computerized tomography, we found that the maturation process occurred gradually from the outside to the inside of the velamen radicum when observed from longitudinal and transverse perspectives (Fig. 2A, B). Moreover, there was an exponential increase in the proportion of mature cells as the length ratio (l_n:l) increased (Fig. 2C). The average (from six individual root tips) percentage of mature cells at l_1:l where autolysis began was 80 % (Fig. 2C), indicating that the autolysis process makes up a small proportion of the maturation process.

De novo *assembly and comparative analysis of RNA-Seq data*

In total, 491 875 666 raw reads were generated from the three replicates of the distal, middle and proximal thirds. After filtering adapters as well as low-quality sequences, we observed a total of 479 757 230 clean reads in the three sections. The six libraries generated 71.96 Gb of clean bases, the base average error rate was 0.03 % and the average Q20 and Q30 values were 97.11 % and 92.29 %, respectively. The average GC content was 46.78 % (Supplementary data Table S2). A total of 302 669 695 transcripts were generated with an average length of 1135 bp based on Trinity software. We then assembled 161 444 unigenes whose length distribution ranged from 201 to 17 618 bp. Among the transcripts, the N50 and N90 values were 2267 and 400 bp, respectively, whereas the values were 2424 and 591 bp among the unigenes (Supplementary data Table S3). The sequencing data were uploaded to the Sequence Read Archive (SRA) of the NCBI under accession numbers SRR9610213, SRR9610220, SRR9610221, SRR9610309, SRR9610311, SRR9610313, SRR9610315, SRR9610316 and SRR9610317.

Functional annotation and analysis of differentially expressed genes

In total, the transcriptome sequencing of all nine samples resulted in the annotation of 117 090 unigenes, accounting for 59.07 % of all unigenes in the Nr database (Supplementary data Table S4). A total of 60.5 % exhibited close homology with sequences of *Dendrobium catenatum*, followed by *Phalaenopsis equestris* (21.8 %), *Apostasia shenzhenica* (2.6 %), *Ricinus communis* (1.0 %) and *Elaeis guineensis* (0.8 %) (Supplementary data Fig. S1a).

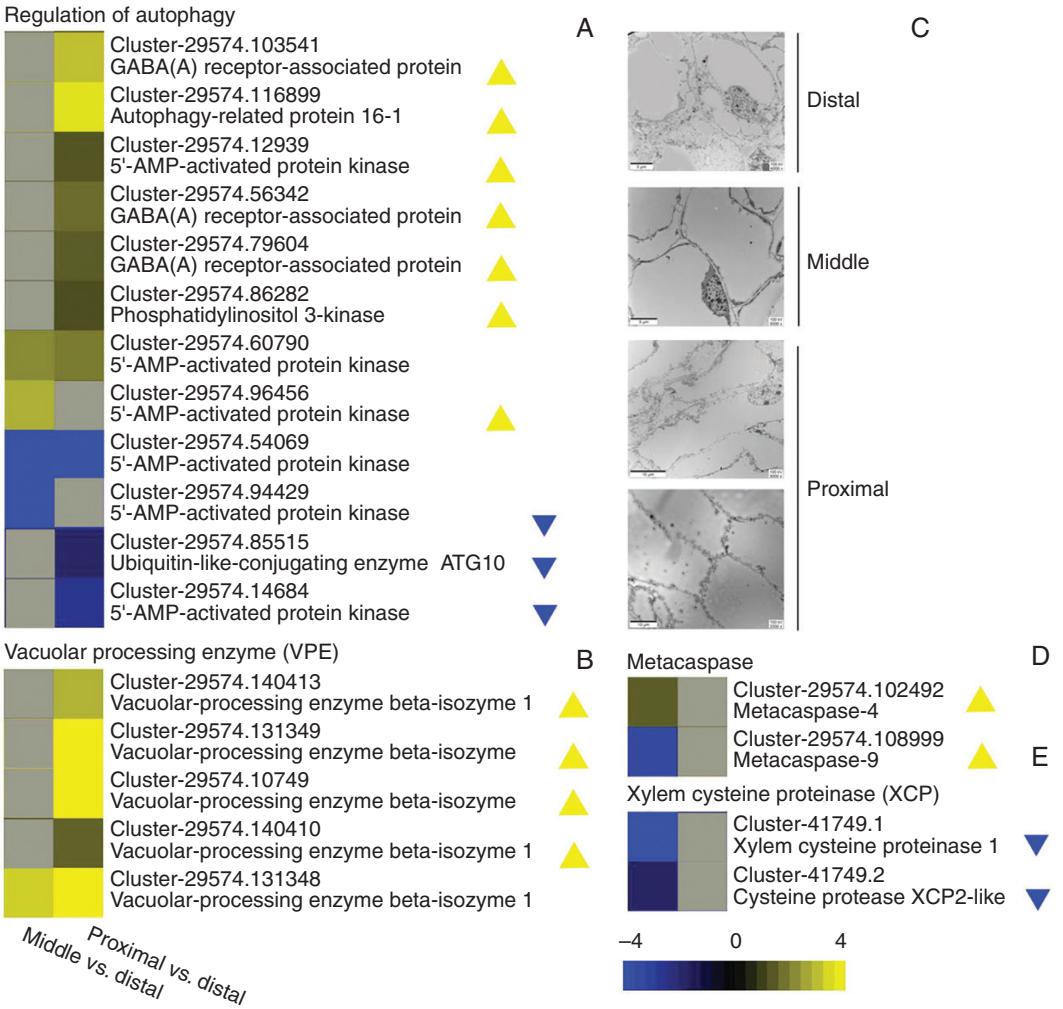

FIG. 4. Changes in expression of transcripts involved in programmed cell death (PCD) and anatomy of cell death. (A) Expression heat maps for transcripts mapped to regulation of autophagy; (B) expression heat maps for vacuolar processing enzyme (VPE); (C) TEM observation of cells of the velamen radicum from three parts of the root tip (i.e. the distal third, middle third and proximal third); (D) expression heat maps for metacaspase; (E) expression heat maps for xylem cysteine proteinase (XCP) detected through differentially expressed gene analysis. Yellow or blue represents upregulated or downregulated, grey with yellow or blue arrowheads indicates that the genes were upregulated or downregulated, but the P_{adj} was ≥0.05. The scale bar represents the $\log_2$ fold change in differentially expressed genes.

We identified a total of 4273 DEGs in the comparison of the middle and distal third of the root tip, comprising 1679 upregulated and 2594 downregulated DEGs. We identified 874 DEGs in the comparison of the proximal third and distal third, comprising 517 upregulated and 357 downregulated DEGs. Finally, we identified 7140 DEGs in the comparison of the proximal third and middle third, comprising 3197 upregulated and 3943 downregulated DEGs (Supplementary data Fig. S2a–c). In addition, the DEG clustering constructed using the k_{means} method revealed ten sub-clusters (Supplementary data Fig. S3). The comparative analysis between the middle third vs. the distal third, the proximal third vs. the distal third and the proximal third vs. the middle third transcriptomes showed that the transcription of 1515 DEGs were only detectable in the middle third vs. the distal third, 4005 DEGs were only detectable in the proximal third vs. the distal third and 205 DEGs were only detectable in the proximal third vs. the middle third; 124 DEGs were common to all detections from the comparison groups (Supplementary data Fig. S1b). The expression patterns of all the selected genes were consistent with the results of the RNA-Seq analysis (Supplementary data Fig. S4), suggesting that our transcriptomic data are valid and reliable.

Regulatory genes related to programmed cell death of the velamen radicum

We compared the differences in the expression of genes likely to be involved in initiation of PCD of the velamen radicum. Subclasses of the NAC-domain proteins play an important role in PCD of the xylem (Kubo *et al.*, 2005; Ko *et al.*, 2006; Zhong *et al.*, 2006; Ohashi-Ito *et al.*, 2010). We subjected all unigenes to analysis of potential NAC-domain proteins, finding 32 genes belonging to sub-classes of NAC-domain

proteins, which might qualify as candidates for the master switches during development of the velamen radicum (Table 1). Several hormones were involved in inducing xylem cell death, with brassinosteroids and ethylene being the most important (Yamamoto *et al.*, 1997; Pesquet and Tuominen, 2011; Du *et al*., 2020). We mapped a total of eight genes to the signalling pathways of brassinosteroids and ethylene. Among these genes, that encoding the ethylene receptor (ETR) located in the endoplasmic reticulum was upregulated in the middle third compared with the distal third of the velamen radicum (Fig. 5). We found that four of five genes related to respiratory-burst NADPH oxidase and two catalase isozymes were upregulated with the development of the velamen radicum cells, while two superoxide dismutases were downregulated in both the middle and proximal third compared with the distal third (Fig. 6).

Cellulose, lignin, cutin and suberin are thought to be involved in the patterning of the secondary cell wall, with cellulose synthase being the principal enzyme in the process of cellulose biosynthesis (Oda *et al.*, 2005; Lacayo *et al.*, 2010; Carteni *et al*., 2014). We found 37 genes that were the subunits of cellulose synthase; compared with the distal third, 33 genes were upregulated in the middle third or proximal third (Fig. 3B). Cytoskeleton-related factors are possibly involved in pre-defining the architecture of secondary cell wall thickening; cortical microtubules localize the cellulose synthase complexes at the edges of secondary cell wall thickenings (Taylor *et al.*, 2000), and we found 37 genes differentially expressed as microtubule-associated proteins during the development of the velamen radicum (Supplementary data Fig. S5). Given that phenylpropanoid is the monomer of lignin, we found 149 genes mapped to the phenylpropanoid biosynthesis pathway. Among them, phenylalanine ammonia lyase (PAL) is the principal enzyme of biosynthesis of phenylpropanoid, of which the eight genes we identified as responsible were all upregulated during the process of maturation. Cinnamyl-alcohol dehydrogenase (CAD) and ferulate-5-hydroxylase (F5H) are also important enzymes in biosynthesis, and these showed similar trends of expression to PAL (Fig. 7). We also found that six genes mapped to cutin biosynthesis were upregulated (Supplementary data Fig. S6).

The final step of PCD of the velamen radicum cell is to initiate cell death and autolysis. Cytoplasmic degradation by autophagy is likely to be fundamental for plant PCD. Indeed, we found that eight of 12 genes mapped to the regulation of autophagy were upregulated in the middle or proximal third compared with the distal third of the velamen radicum (Fig. 4A). VPE contributes to vacuolar collapse, and we found five genes responsible for VPE that were all upregulated during PCD in the middle or proximal third compared with the distal third (Fig. 4B). Metacaspases are a class of cell death-associated proteases; compared with the distal third, two metacaspases were upregulated in the middle third or proximal third (Fig. 4D).

DISCUSSION

We have described in detail the maturation process of the velamen radicum in the roots of epiphytic orchids, showing that it is an example of developmental PCD (Pridgeon, 1987). By using TEM and light microscopy, we found that cell and vacuole size increased, DNA degraded, the cytoplasm and organelles decreased, the vacuoles ruptured and cell walls thickened with the development of the velamen radicum. These are the anatomical features of typical autophagic PCD (van Doorn and Woltering, 2005). According to longitudinal and transverse perspectives using X-ray micro-computerized tomography, we showed that the final process of autolysis occurred gradually but exponentially from the outside to the inside of the velamen radicum. Changes in the expression of genes encoding cytoskeleton-controlled cellulose synthase complexes, PAL, VPE, cysteine proteases and metacaspase in particular indicate that these processes play important roles in molecular control of the processes: initiation of PCD, formation of the secondary cell wall and execution of autolysis in velamen radicum development (Fig. 8).

Initiation of programmed cell death

As we hypothesized that the developmental process of the velamen radicum is similar to that of xylem vessels and fibres, we investigated DEGs of sub-classes of NAC-domain proteins that could be candidates for the master switches of developmental PCD in the velamen radicum. Transcription factors belonging to NAC-domain proteins control the transformation of xylem cell differentiation (Kubo *et al.*, 2005; Mitsuda *et al.*, 2005; Ko *et al.*, 2006; Zhong *et al.*, 2006). Among them, VND6 and VND7, both of which are preferentially expressed in their potential vessel cells (Kubo *et al.*, 2005), have been found to induce the differentiation of metaxylem and protoxylem vessels. In contrast, secondary wall-associated NAC-domain protein 1 (SND1) is involved in the differentiation of fibre cells (Mitsuda *et al.*, 2005; Ko *et al.*, 2006). A series of transcription factors play an important role downstream of SND1, and ultimately lead to the formation of the secondary cell wall (Zhong *et al.*, 2007, 2008; Zhou *et al.*, 2009). We were not able to identify transcription factors of VND6, VND7 or SND1, but we found 32 genes belonging to sub-classes of NAC-domain proteins (Table 1).

Brassinosteroids and ethylene are among the most important plant hormones involved in the initiation of xylem cell death. Brassinosteroids have been discovered to be involved in cell differentiation of *Zinnia elegans* cells (Yamamoto *et al.*, 2001; Du *et al*., 2020), and vessel differentiation has also been successfully triggered in cell suspension (Kubo *et al.*, 2005) and tissue culture (Kwon *et al.*, 2010) of *Arabidopsis thaliana* via the addition of brassinolide, a synthetic brassinosteroid. Furthermore, expression of genes associated with PCD was not observed when *Z. elegans* cells were treated with an inhibitor of brassinosteroid synthesis (Yamamoto *et al.*, 1997). Consequently, brassinosteroids have been thought to regulate vessel differentiation (Yamamoto *et al*., 1997, 2001; Kubo *et al.*, 2005), or to initiate vessel PCD (Kwon *et al.*, 2010). Moreover, brassinosteroids could affect the thickening patterns of vascular bundle cell walls (Ibanes *et al*., 2009; Carlsbecker *et al.*, 2010; Fabregas *et al*., 2010). Although we found that seven genes mapped to the brassinosteroid signalling pathway, the expression patterns were not identical, which might indicate that brassinosteroid signalling in the velamen radicum was not specific to PCD (Fig. 5).

TABLE 1. *Differentially expressed NAC-domain-containing protein genes between the middle and distal third, the proximal and distal third, and the proximal and middle third.*

Gene_id	Gene length	NR ID	NR score	NR description	Species	UP/DOWN (middle vs.distal, proximal vs. distal, proximal vs. middle)			Log_2FC (middle vs.distal, proximal vs. distal, proximal vs. middle)			*q*-value (middle vs.distal, proximal vs. distal, proximal vs. middle)		
Cluster-29574.134052	1419	XP_020699447.1	1297	NAC-domain-containing protein 92-like	*Dendrobium catenatum*	UP	UP	FALSE	3.2334	2.6226	-0.5867	5.29E-06	8.61E-08	0.99999
Cluster-29574.37530	1666	PKU66917.1	1337	NAC-domain-containing protein 100	*Dendrobium catenatum*	UP	UP	FALSE	4.8094	6.4248	1.6564	2.12E-08	3.17E-36	0.99999
Cluster-29574.18007	1180	XP_020588134.1	1157	Uncharacterized protein LOC110029961 isoform X1	*Phalaenopsis equestris*	DOWN	FALSE	UP	-6.0841	0.7254	6.8358	0.007412	0.935	0.013675
Cluster-29574.61	1248	PKU76773.1	1433	NAC-domain-containing protein 8	*Dendrobium catenatum*	FALSE	UP	FALSE	3.1516	6.988	3.9042	0.9643	5.60E-05	0.21777
Cluster-29574.37656	1550	XP_020591672.1	895	NAC-domain-containing protein 83-like	*Phalaenopsis equestris*	UP	FALSE	FALSE	8.6396	22.346	-0.3089	2.01E-05	NA	NA
Cluster-29574.37657	1463	XP_020591672.1	935	NAC-domain-containing protein 83-like	*Phalaenopsis equestris*	FALSE	UP	FALSE	2.9346	3.5558	0.66018	0.078502	0.00349	0.99999
Cluster-29574.40630	1889	XP_020699012.1	1024	NAC-domain-containing protein 92-like	*Dendrobium catenatum*	FALSE	UP	FALSE	4.1318	5.8579	1.7644	0.077827	0.000758	0.89349
Cluster-29574.138595	1726	PKU63584.1	1227	NAC-domain-containing protein 100	*Dendrobium catenatum*	FALSE	UP	FALSE	0.74571	3.3046	2.5967	0.98429	0.003748	0.33626
Cluster-29574.138596	2101	XP_020692471.1	779	NAC-domain-containing protein 92-like	*Dendrobium catenatum*	FALSE	UP	FALSE	1.4119	3.4498	2.0784	0.52243	0.000457	0.90163
Cluster-29574.111339	1750	XP_020680837.1	1715	NAC-domain-containing protein 73-like isoform X3	*Dendrobium catenatum*	FALSE	DOWN	FALSE	-5.1784	-4.829	0.3526	0.15105	0.036308	0.99999
Cluster-29574.111338	1639	XP_020680837.1	1721	NAC-domain-containing protein 73-like isoform X3	*Dendrobium catenatum*	DOWN	FALSE	FALSE	-4.8184	-3.44	1.401	0.010128	0.24349	0.99999
Cluster-29574.117582	1428	BAF36563.1	1654	NAC-domain protein	*Cymbidium* hybrid cultivar	FALSE	UP	FALSE	1.7088	3.8067	2.1082	0.73259	0.021427	0.99999
Cluster-37048.0	1408	XP_020692881.1	1183	NAC-domain-containing protein 37-like	*Dendrobium catenatum*	FALSE	UP	UP	1.2872	9.1989	7.936	0.98898	0.001366	0.018987
Cluster-29574.45662	629	XP_020693933.1	974	NAC-domain-containing protein 100-like	*Dendrobium catenatum*	UP	UP	FALSE	1.9614	2.1607	0.23019	0.007608	0.020612	0.99999
Cluster-29574.45663	1673	XP_020693932.1	1450	NAC-domain-containing protein 100-like	*Dendrobium catenatum*	UP	FALSE	FALSE	2.0649	1.4565	-0.5881	0.001065	0.20515	0.99999
Cluster-29574.10775	1302	PKU69540.1	1110	NAC-domain-containing protein 8	*Dendrobium catenatum*	UP	UP	FALSE	8.4166	12.191	3.7899	0.003082	6.07E-09	0.37167
Cluster-29574.79590	1538	XP_020693932.1	1450	NAC-domain-containing protein 100-like	*Dendrobium catenatum*	UP	UP	FALSE	2.6265	2.6532	0.05908	0.01445	0.012796	0.99999

TABLE 1. Continued

Gene_id	Gene length	NR ID	NR score	NR description	Species	UP/DOWN (middle vs.distal, proximal vs. distal, proximal vs. middle)			Log_2FC (middle vs.distal, proximal vs. distal, proximal vs. middle)			*q*-value (middle vs.distal, proximal vs. distal, proximal vs. middle)		
Cluster-29574.122616	1440	BAF36563.1	1654	NAC-domain protein	*Cymbidium* hybrid cultivar	FALSE	UP	FALSE	1.5724	3.749	2.1889	0.79548	0.000134	0.75751
Cluster-11181.0	1026	PKU85873.1	1050	NAC-domain-containing protein 100	*Dendrobium catenatum*	FALSE	UP	UP	NA	10.174	9.8701	NA	1.52E-06	3.74E-05
Cluster-29574.9733	1576	XP_020676606.1	1124	NAC-domain-containing protein 73-like	*Dendrobium catenatum*	UP	UP	FALSE	5.41	9.5308	4.1456	0.008722	2.77E-10	0.053026
Cluster-29574.122342	2103	XP_020672393.1	1722	NAC-domain-containing protein 10-like	*Dendrobium catenatum*	FALSE	FALSE	UP	-1.5985	1.2956	2.9096	0.54008	0.47313	0.035957
Cluster-29574.6184	3196	XP_020685794.1	1911	Uncharacterized protein LOC110102005 isoform X2	*Dendrobium catenatum*	DOWN	FALSE	FALSE	-6.6759	-0.829	5.8426	0.010232	0.97969	0.99999
Cluster-29574.91591	2233	PKU70851.1	1437	NAC-domain-containing protein 2	*Dendrobium catenatum*	UP	UP	FALSE	2.122	2.2453	0.1377	0.01938	2.88E-06	0.99999
Cluster-29574.136707	3914	PKU71267.1	288	Protein BEARSKIN1	*Dendrobium catenatum*	FALSE	FALSE	UP	-3.3392	2.7905	6.2552	0.98898	0.76792	0.002118
Cluster-29574.109590	3172	XP_020690811.1	288	NAC-domain-containing protein 72-like	*Dendrobium catenatum*	FALSE	FALSE	UP	-4.4633	2.44	6.9385	0.97775	0.82209	0.007624
Cluster-29574.143585	1501	XP_020675944.1	1541	NAC-domain-containing protein 100-like	*Dendrobium catenatum*	FALSE	UP	UP	-1.4628	3.2697	4.7699	0.68981	0.000229	0.000948
Cluster-29574.143583	2374	XP_020594160.1	777	NAC-domain-containing protein 100-like	*Phalaenopsis equestris*	FALSE	FALSE	UP	-2.8202	2.7162	5.4967	0.97793	0.35373	0.030797
Cluster-29574.37527	1179	XP_020699012.1	553	NAC-domain-containing protein 92-like	*Dendrobium catenatum*	UP	UP	FALSE	3.0521	5.028	2.0129	0.000132	1.74E-07	0.42721
Cluster-29574.100799	1099	XP_020693359.1	752	NAC-domain-containing protein 83-like, partial	*Dendrobium catenatum*	FALSE	UP	FALSE	2.9967	3.2135	0.22641	0.06431	0.031761	0.99999
Cluster-29574.137993	1441	PKU66917.1	1472	NAC-domain-containing protein 100	*Dendrobium catenatum*	UP	FALSE	FALSE	3.9181	2.6357	-1.2467	0.043809	0.21134	0.99999
Cluster-29574.7144	1374	XP_020577921.1	636	SUPPRESSOR OF GAMMA RESPONSE 1-like	*Phalaenopsis equestris*	FALSE	UP	UP	-2.4774	6.1453	8.6682	0.98898	2.50E-06	1.79E-05
Cluster-29574.32266	1145	XP_020591672.1	174	NAC-domain-containing protein 83-like	*Phalaenopsis equestris*	FALSE	UP	FALSE	2.1829	2.3607	0.19915	0.11446	0.025244	0.99999

See Fig. 1 for the definitions of distal, middle and proximal.

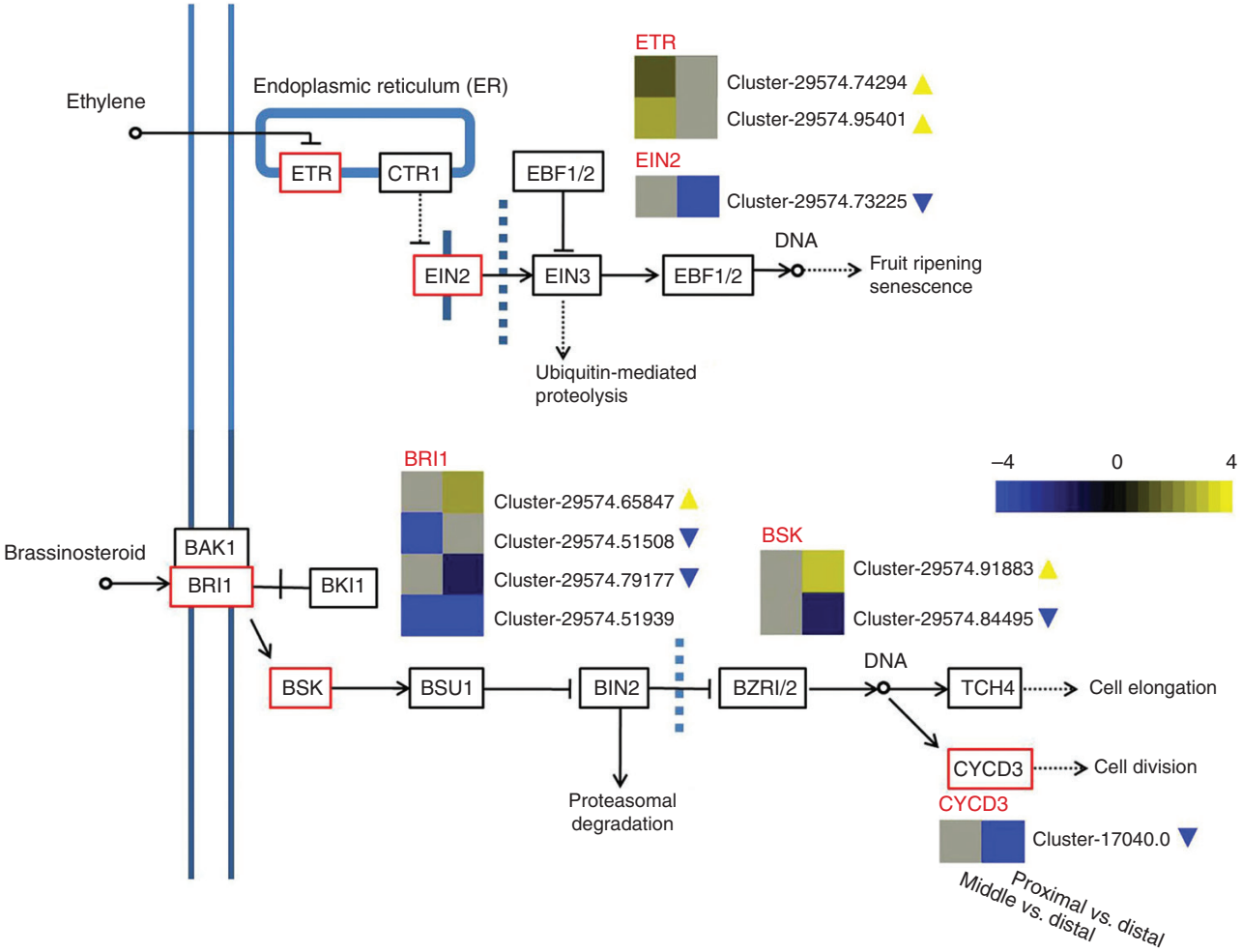

FIG. 5. Differentially expressed genes were mapped to brassinosteroid and ethylene signal transduction pathways in the KEGG database. Yellow or blue represents upregulated or downregulated, grey with yellow or blue arrowheads indicates that the genes were upregulated or downregulated, but the P_{adj} was ≥0.05. The scale bar represents the $\log_2$ fold change in differentially expressed genes.

Ethylene participates in regulation of developmental and inducible forms of cell death, such as during senescence and aerenchyma formation (Wang *et al.*, 2002), and it can control the signalling of PCD at the early and late stages during vessel differentiation (Pesquet and Tuominen, 2011; Pesquet *et al.*, 2013). Among the ethylene signalling pathway genes, we found that the ETR (located in the endoplasmic reticulum) was upregulated during development of the velamen radicum (Fig. 5). Nitric oxide, which links ethylene signalling to cell death, is a bioactive signal factor contributing to processes related to secondary cell wall lignifications during PCD (Gabaldon *et al.*, 2005; Gomez Ros *et al.*, 2006). It has been suggested that transcription factors and the activity of some of the enzymes in lignin biosynthesis are possible targets of nitric oxide action (Gabaldon *et al.*, 2005; Gomez Ros *et al.*, 2006).

Formation of the secondary cell wall

Cellulose and lignin are the main components involved in the process of thickening of the secondary cell wall of xylem vessels and fibres (Oda *et al.*, 2005; Lacayo *et al.*, 2010; Carteni *et al.*, 2014). We also observed, using TEM and light microscopy, that cell walls of the velamen radicum were thickened at the final stage of development, which probably occurred via the accumulation of cellulose and lignin (Fig. 4A). Cytoskeleton-related factors controlling the orientation of deposited cellulose microfibrils (Paredez *et al.*, 2006; Wightman and Turner, 2008) have been hypothesized to be involved in pre-defining the architecture of thickening of the secondary cell wall. Among them, microtubule-associated proteins are also essential for the localization and patterning of the secondary cell wall in the vessels formed from differentiating *A. thaliana* cells (Oda *et al.*, 2005; Lacayo *et al.*, 2010; Carteni *et al.*, 2014). Fukuda (1987) also reported changes in tubulin synthesis and of the genes encoding tubulin during vessel differentiation,. We found that 25 genes coding for microtubule-associated protein (Supplementary data Fig. S5) and 12 genes coding for tubulin (Supplementary data Fig. S7) were upregulated during the development of the velamen radicum. In addition, cortical microtubules, located beneath the plasma membrane, delineated the formation of the secondary cell wall

in xylem vessels by localizing cellulose synthase complexes, which are the main enzymes associated with cellulose synthesis (Baskin, 2001). We observed 37 genes in total as the sub-units for cellulose synthase; compared with the distal third of the root tip, 33 genes were upregulated in the middle and proximal third (Fig. 3B). All of these changes indicate that cytoskeleton-controlled cellulose involved in the formation of the secondary cell wall is an important part of the process of PCD in the velamen radicum. This is also consistent with previous results showing that cells that would have developed into the velamen radicum have cortical microtubules organized into parallel arrays, and cellulose deposition at that position was associated with changes in the microtubules from an oblique pattern to a bundled and regularly spaced array in the roots of epiphytic orchids (Idris and Collings, 2014).

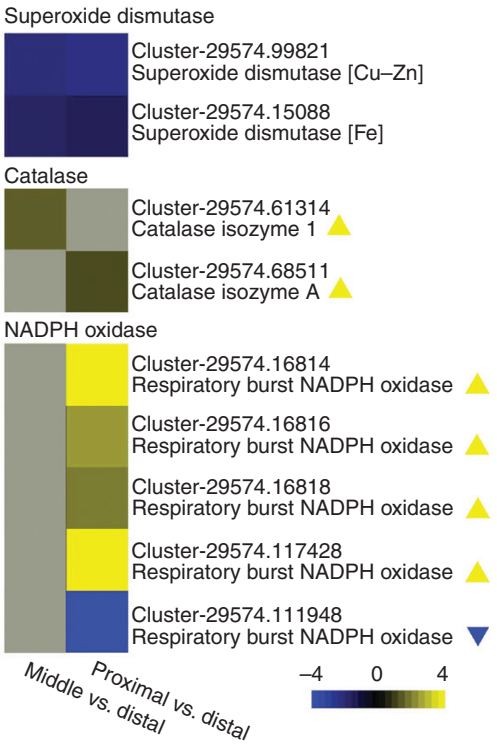

FIG. 6. Expression heat maps for catalase, superoxide dismutase and NADPH oxidase detected through differentially expressed gene analysis. Yellow or blue represents upregulated or downregulated, grey with yellow or blue arrowheads indicates that the genes were upregulated or downregulated, but the P_{adj} was ≥0.05. The scale bar represents the $\log_2$ fold change in differentially expressed genes.

Lignin is one of the largest potential phenylpropanoid carbon sinks in plant tissues (Vogt, 2010), and we found 149 genes mapped to the phenylpropanoid biosynthesis pathway (Fig. 7). Phenylpropanoid metabolism relies on PAL via phenylalanine deamination (Kao *et al.*, 2002). We found that eight genes involved in PAL were all upregulated during the development of the velamen radicum. Cinnamyl alcohol dehydrogenase (CAD) is an NADPH-dependent enzyme, reducing derivatives from phenylpropenyl aldehyde, with the latter mainly becoming precursors of lignins and lignans (Anterola and Lewis, 2002). We determined that genes coding for CAD had similar trends of expression to PAL, being upregulated compared with the distal third (Fig. 7). Stewart (2009) found that overexpression of F5H led exclusively to a change to syringyl-lignin, suggesting an important role for F5H in the structure and physical functioning of lignin. We also observed upregulated trends of F5H during velamen radicum development (Fig. 7). Early H_2O_2 synthesis in living cells has been suggested as necessary for lignification in the earlier and later stages of secondary cell wall formation; H_2O_2 synthesis is also involved in the peroxidase-mediated oxidative polymerization of cinnamyl alcohols to lignin (Liu *et al.*, 1999). We found that four of five genes of respiratory-burst NADPH oxidase and two catalase isozymes were upregulated during the development of cells from the velamen radicum (Fig. 6), possibly helping in the formation of the secondary cell wall in the velamen radicum.

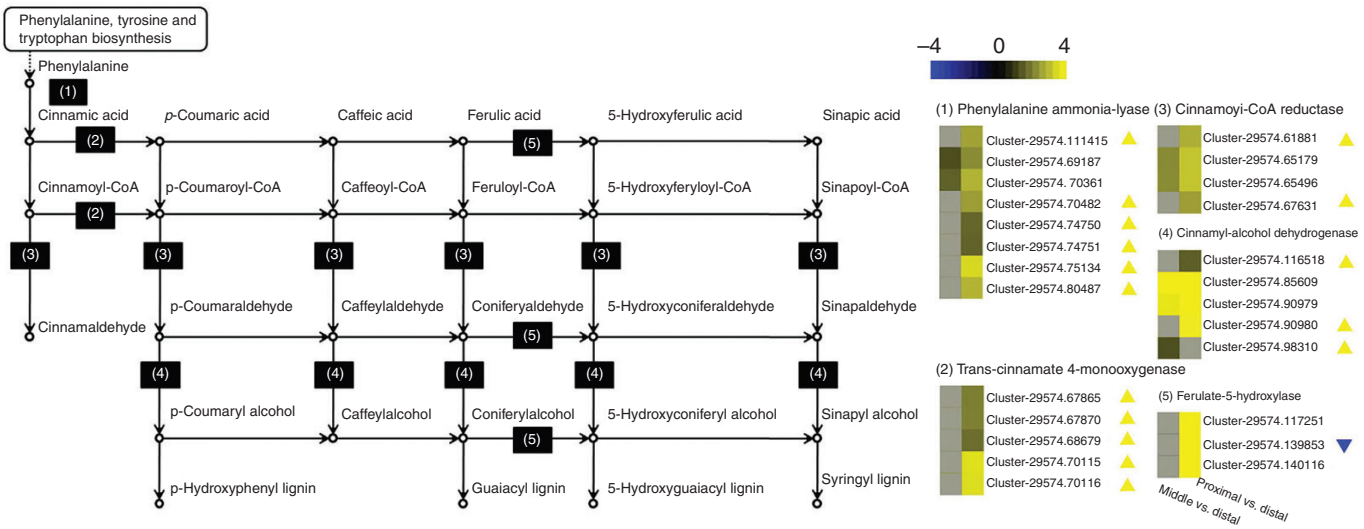

FIG. 7. Differentially expressed genes were mapped to phenylpropanoid biosynthesis signal transduction pathways in the KEGG database. Yellow or blue represents upregulated or downregulated, grey with yellow or blue arrowheads indicates that the genes were upregulated or downregulated, but the P_{adj} was ≥0.05. The scale bar represents the $\log_2$ fold change in differentially expressed genes.

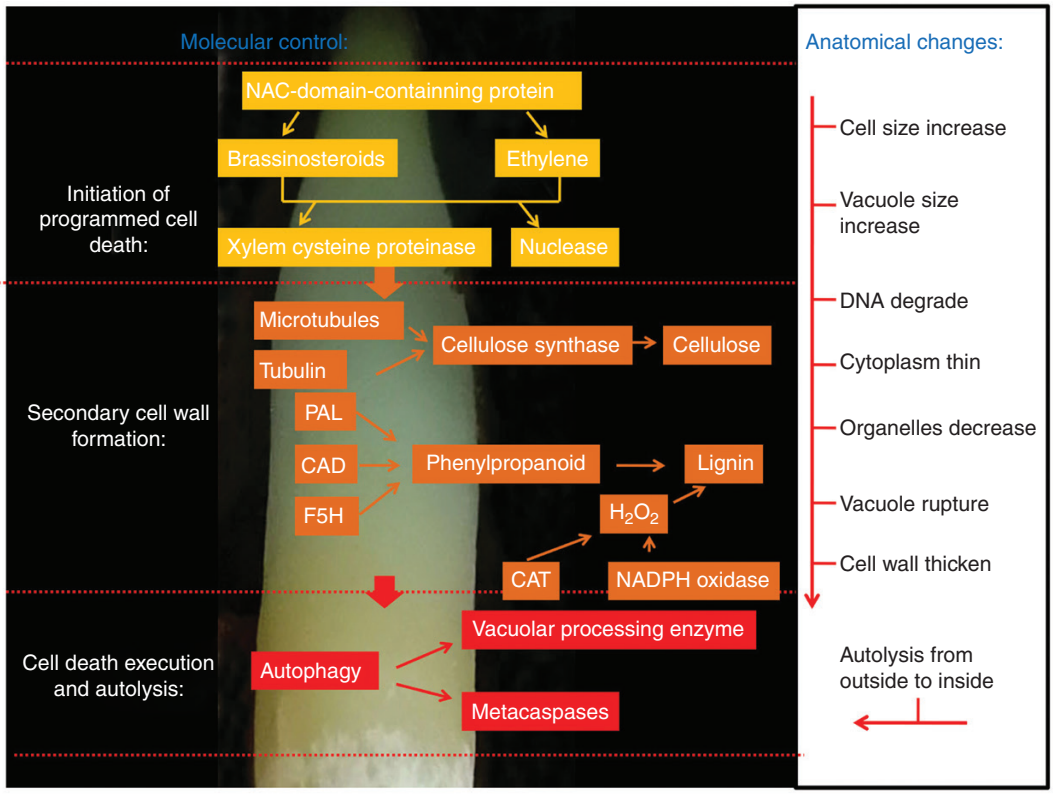

FIG. 8. Proposed diagrammatic representation of developmental programmed cell death in the velamen radicum. CAD, cinnamyl-alcohol dehydrogenase; CAT, catalase; F5H, ferulate-5-hydroxylase; PAL, phenylalanine ammonia lyase.

Execution of cell death and autolysis

By light microscopy and TEM, we observed gradual enlargement and finally rupture of the vacuoles (Fig. 4C). It has been previously suggested that the final stage of PCD comprises two tightly linked phases: (1) execution of cell death and (2) autolysis (Ruzicka *et al*., 2015), with vacuolar integrity typically playing a central role in controlling these two processes of autophagic PCD (Fukuda, 1997; Obara *et al.*, 2001; van Doorn and Woltering, 2005; Courtois-Moreau *et al.*, 2009; Iakimova and Woltering, 2017).

With the rupture of the vacuolar membrane, the onset of autophagy is typical in the final phase of developmental PCD. Due to such rupture, a lot of hydrolases leak into the cytoplasm, resulting in complete degradation of the cytoplasm and cell walls in some cases (Matile and Winkenbach, 1971; Fukuda, 1997). Nevertheless, autophagic mechanisms have been suggested to accelerate death or to reduce the chances of death, meaning a dual function of autophagy in regulating PCD. In *A. thaliana*, knockout mutations of autophagy genes lead to early leaf senescence, meaning that autophagy does not promote PCD but instead protects the cells against it (Liu and Bassham, 2012). In contrast, autophagy is required for the PCD in cells induced by hormones and differentiated into xylem (Kwon *et al.*, 2010). Autophagy-related (ATG)-8 is central in the regulation of autophagy, adhering to the developing autophagic membranes by lipidation (Li and Vierstra, 2012). We found that ubiquitin-like conjugating enzyme ATG-10 was downregulated in the proximal third compared with the distal third of the velamen radicum (Fig. 4A). ATG-10 connects ATG-12 to ATG-5 via an isopeptide bond assembled by a parallel conjugation pathway involving ATG-8 (Li and Vierstra, 2012). Moreover, nine of 12 genes mapped to the regulation of autophagy were upregulated during the development of the velamen radicum, possibly indicating the dual role of autophagy in the process.

It has been assumed that VPE is one of the hallmarks of autophagic PCD because it emerges in almost all known forms of the process (van Doorn and Woltering, 2005; van Doorn *et al.*, 2011). Indeed, VPE plays a role in the post-translational modification of a variety of vacuolar proteins, and it might contribute to vacuolar collapse during cell death in xylem vessels (Hatsugai *et al.*, 2015). During secondary development of fibres, Courtois-Moreau (2009) also demonstrated upregulation of VPE. We determined that five genes coding for this enzyme were all upregulated preceding PCD of the velamen radicum (Fig. 4B). As such, determining the possible involvement of VPE in the process will clarify the control of PCD in the velamen radicum.

Through X-ray micro-computerized tomography, we clearly observed that the final process of autolysis occurred gradually from the outside to the inside of the velamen radicum (Fig. 2). Several hydrolytic activities contribute to this process, including detected activity from endonucleases (Thelen and Northcote, 1989; Aoyagi *et al.*, 1998), several RNases (Thelen and Northcote, 1989; Ye and Droste, 1996) and proteases (Beers and Freeman, 1997; Woffenden *et al.*, 1998). Among them, cysteine proteases are thought to be the main

executors of cellular autolysis (Minami and Fukuda, 1995; Funk *et al.*, 2002; Avci *et al.*, 2008; Bollhoner *et al.*, 2012). *Arabidopsis thaliana* xylem cysteine proteinase 1 (XCP1) and XCP2, localized mainly to the vacuole, are specifically expressed in vessels (Zhao *et al.*, 2000; Funk *et al.*, 2002). During root vessel differentiation, both XCP1 and XCP2 participate in cytostromatic micro-autolysis before vacuole rupture and in protoplast mega-autolysis after vacuole rupture (Avci *et al.*, 2008). We also found one xylem cysteine proteinase downregulated in the middle third compared with the distal third of the velamen radicum (Fig. 4E). Metacaspases are plant cell death-linked proteases which are structurally similar to animal caspases (Suarez *et al.*, 2004; He *et al.*, 2008). The loss of function of xylem-specific *A. thaliana* metacaspase 9 (AtMC9) leads to defects in vessels and the post-mortem autolysis of vessels (Bollhöner *et al.*, 2012). During the latter stages of xylem maturation in *Populus*, upregulation of a homologue of AtMC9 occurs (Courtois-Moreau *et al.*, 2009). Bollhöner *et al.* (2012) examined the potential linkage of AtMC9 and XCP1/XCP2, showing that XCP2 appears as a target of AtMC9 *in vitro*, and after analysing the triple mutant *atmc*9 *xcp*1 *xcp*2, showed that AtMC9 regulates the activity of several unidentified, papain-like cysteine proteases (Bollhöner *et al.*, 2012). We found that two metacaspases were upregulated in the middle third or the proximal third compared with the distal third (Fig. 4D), which could implicate metacaspase in PCD of the velamen radicum.

Conclusions

We have determined that the process of PCD of the velamen radicum in epiphytic orchids includes three tightly linked steps: (1) initiation of PCD; (2) formation of the secondary cell wall; and (3) execution of autolysis following cell death (Fig. 8). During initiation of PCD, we found several genes involved in brassinosteroid and ethylene signalling pathways which may play major roles. For the formation of the secondary cell wall during the process of PCD, cytoskeleton-controlled cellulose biosynthesis is an essential precursor, and lignin governed by PAL and NADPH oxidase are also important components. We also discovered that the process of cell autolysis in the velamen radicum is rapid, and the regulation of autophagy, VPE, cysteine proteases and metacaspase are likely to play an important role in the final execution of cell death and autolysis. These results therefore improve our understanding of the specific progress of this process involved in developmental PCD in the velamen radicum of epiphytic orchids. Further research, based on investigation of how the process of developmental PCD changes with the environmental conditions, is still required to understand the mechanisms underlying ecological adaptations of epiphytic orchids.

SUPPLEMENTARY DATA

Supplementary data are available online at https://academic.oup.com/aob and consist of the following. Figure S1: species classification and unigenes specific to the middle third vs. the distal third, the proximal third vs. the distal third and the proximal third vs. the middle third. Figure S2: global distributions. Figure S3: clustering of differentially expressed genes constructed using the k_{means} method. Figure S4: expression patterns of qRT-PCR from six selected genes. Figure S5: expression heat maps for microtubule-associated protein. Figure S6: differentially expressed genes were mapped to cutin biosynthesis signal transduction pathways in the KEGG database. Figure S7: expression heat maps for tubulin. Table S1: DEGs and primers used for qRT-PCR validation of the transcriptomes. Table S2: summary statistics relating to the RNA-Seq libraries derived from the distal, middle and proximal third. Table S3: statistical report of unigenes from the transcriptome assembly. Table S4: summary of annotations of the unigenes in the transcriptome.

ACKNOWLEDGEMENTS

We are grateful to Jin Xu (Xishuangbanna Tropical Botanical Garden, Chinese Academy of Sciences) and An-Dan Zhu (Kunming Institute of Botany, Chinese Academy of Sciences) for their useful suggestions for our experiment.

FUNDING

This work was supported by the Strategic Priority Research Program of the Chinese Academy of Sciences (grant no. XDB31000000), the National Natural Science Foundation of China (grant no. 31901092, 31670342, 31870385), open funding from CAS Key Laboratory of Tropical Forest Ecology to JWL, and the Science and Technology Plan of Yunnan (grant no. 2018BB010).

LITERATURE CITED

Anterola AM, Lewis NG. 2002. Trends in lignin modification: a comprehensive analysis of the effects of genetic manipulations/mutations on lignification and vascular integrity. *Phytochemistry* **61**: 221–294.

Aoyagi S, Sugiyama M, Fukuda H. 1998. BEN1 and ZEN1 cDNAs encoding S1-type DNases that are associated with programmed cell death in plants. *FEBS Letters* **429**: 134–138.

Avci U, Earl Petzold H, Ismail IO, Beers EP, Haigler CH. 2008. Cysteine proteases XCP1 and XCP2 aid micro-autolysis within the intact central vacuole during xylogenesis in *Arabidopsis* roots. *The Plant Journal* **56**: 303–315.

Aybeke M. 2012. Comparative anatomy of selected rhizomatous and tuberous taxa of subfamilies Orchidoideae and Epidendroideae (Orchidaceae) as an aid to identification. *Plant Systematics and Evolution* **298**: 1643–1658.

Baskin TI. 2001. On the alignment of cellulose microfibrils by cortical microtubules: a review and a model. *Protoplasma* **215**: 150–171.

Bassham DC, Laporte M, Marty F, *et al.* 2006. Autophagy in development and stress responses of plants. *Autophagy* **2**: 2–11.

Beers EP, Freeman TB. 1997. Proteinase activity during tracheary element differentiation in *Zinnia* mesophyll cultures. *Plant Physiology* **113**: 873–880.

Benzing DH, Ott DW, Friedman WE. 1982. Roots of *Sobralia macrantha* (Orchidaceae): structure and function of the velamen radicum–exodermis complex. *Amerian Journal of Botany* **69**: 608–614.

Bollhöner B, Prestele J, Tuominen H. 2012. Xylem cell death: emerging understanding of regulation and function. *Journal of Experimental Botany* **63**: 1081–1094.

Bozhkov PV, Filonova LH, Suarez MF. 2005. Programmed cell death in plant embryogenesis. *Current Topics in Developmental Biology* **67**: 135–179.

Carlsbecker A, Lee JY, Roberts CJ, *et al.* 2010. Cell signalling by microRNA165/6 directs gene dose-dependent root cell fate. *Nature* **465**: 316–321.

Cartenì F, Giannino F, Schweingruber FH, Mazzoleni S. 2014. Modelling the development and arrangement of the primary vascular structure in plants. *Annals of Botany* **114**: 619–627.

Chomicki G, Bidel LP, Ming F, *et al.* 2015. The velamen protects photosynthetic orchid roots against UV-B damage, and a large dated phylogeny implies multiple gains and losses of this function during the Cenozoic. *New Phytologist* **205**: 1330–1341.

Courtois-Moreau CL, Pesquet E, Sjödin A, *et al.* 2009. A unique program for cell death in xylem fibers of *Populus* stem. *The Plant Journal* **58**: 260–274.

van Doorn WG, Papini A. 2013. Ultrastructure of autophagy in plant cells: a review. *Autophagy* **9**: 1922–1936.

van Doorn WG, Woltering EJ. 2005. Many ways to exit? Cell death categories in plants. *Trends in Plant Science* **10**: 117–122.

van Doorn WG, Beers EP, Dangl JL, *et al.* 2011. Morphological classification of plant cell deaths. *Cell Death and Differentiation* **18**: 1241–1246.

Du J, Gerttula S, Li Z, *et al.* 2020. Brassinosteroid regulation of wood formation in poplar. *New Phytologist* **225**: 1516–1530.

Escamez S, Tuominen H. 2014. Programmes of cell death and autolysis in tracheary elements: when a suicidal cell arranges its own corpse removal. *Journal of Experimental Botany* **65**: 1313–1321.

Fàbregas N, Ibañes M, Caño-Delgado AI. 2010. A systems biology approach to dissect the contribution of brassinosteroid and auxin hormones to vascular patterning in the shoot of *Arabidopsis thaliana*. *Plant Signaling & Behavior* **5**: 903–906.

Figueroa C, Salazar GA, Zavaleta HA, Engleman EM. 2008. Root character evolution and systematics in Cranichidinae, Prescottiinae and Spiranthinae (Orchidaceae, Cranichideae). *Annals of Botany* **101**: 509–520.

Fukuda H. 1987. A change in tubulin synthesis in the process of tracheary element differentiation and cell-division of isolated *Zinnia* mesophyll-cells. *Plant & Cell Physiology* **28**: 517–528.

Fukuda H. 1997. Tracheary element differentiation. *The Plant Cell* **9**: 1147–1156.

Fukuda H. 2000. Programmed cell death of tracheary elements as a paradigm in plants. *Plant Molecular Biology* **44**: 245–253.

Funk V, Kositsup B, Zhao C, Beers EP. 2002. The *Arabidopsis* xylem peptidase XCP1 is a tracheary element vacuolar protein that may be a papain ortholog. *Plant Physiology* **128**: 84–94.

Gabaldón C, Gómez Ros LV, Pedreño MA, Ros Barceló A. 2005. Nitric oxide production by the differentiating xylem of *Zinnia elegans*. *New Phytologist* **165**: 121–130.

Gómez Ros LV, Paradiso A, Gabaldón C, Pedreño MA, de Gara L, Ros Barceló A. 2006. Two distinct cell sources of H_2O_2 in the lignifying *Zinnia elegans* cell culture system. *Protoplasma* **227**: 175–183.

Grabherr MG, Haas BJ, Yassour M, *et al.* 2011. Full-length transcriptome assembly from RNA-Seq data without a reference genome. *Nature Biotechnology* **29**: 644–652.

Gunawardena AHLAN. 2008. Programmed cell death and tissue remodelling in plants. *Journal of Experimental Botany* **59**: 445–451.

Hatsugai N, Kuroyanagi M, Yamada K, *et al.* 2004. A plant vacuolar protease, VPE, mediates virus-induced hypersensitive cell death. *Science* **305**: 855–858.

Hatsugai N, Yamada K, Goto-Yamada S, Hara-Nishimura I. 2015. Vacuolar processing enzyme in plant programmed cell death. *Frontiers in Plant Science* **6**: 234.

He R, Drury GE, Rotari VI, *et al.* 2008. Metacaspase-8 modulates programmed cell death induced by ultraviolet light and H_2O_2 in *Arabidopsis*. *Journal of Biological Chemistry* **283**: 774–783.

Iakimova ET, Woltering EJ. 2017. Xylogenesis in zinnia (*Zinnia elegans*) cell cultures: unravelling the regulatory steps in a complex developmental programmed cell death event. *Planta* **245**: 681–705.

Ibañes M, Fàbregas N, Chory J, Caño-Delgado AI. 2009. Brassinosteroid signaling and auxin transport are required to establish the periodic pattern of *Arabidopsis* shoot vascular bundles. *Proceedings of the National Academy of Sciences, USA* **106**: 13630–13635.

Idris NA, Collings DA. 2014. Cell wall development in the velamen radicum layer of the orchid *Miltoniopsis* investigated by confocal microscopy. *Malaysian Journal of Microscopy* **10**: 20–26.

Ito J, Fukuda H. 2002. ZEN1 is a key enzyme in the degradation of nuclear DNA during programmed cell death of tracheary elements. *The Plant Cell* **14**: 3201–3211.

Kao YY, Harding SA, Tsai CJ. 2002. Differential expression of two distinct phenylalanine ammonia-lyase genes in condensed tannin-accumulating and lignifying cells of quaking aspen. *Plant Physiology* **130**: 796–807.

Ko JH, Beers EP, Han KH. 2006. Global comparative transcriptome analysis identifies gene network regulating secondary xylem development in *Arabidopsis thaliana*. *Molecular Genetics and Genomics* **276**: 517–531.

Kubo M, Udagawa M, Nishikubo N, *et al.* 2005. Transcription switches for protoxylem and metaxylem vessel formation. *Genes & Development* **19**: 1855–1860.

Kuriyama H. 1999. Loss of tonoplast integrity programmed in tracheary element differentiation. *Plant Physiology* **121**: 763–774.

Kwon SI, Cho HJ, Jung JH, Yoshimoto K, Shirasu K, Park OK. 2010. The Rab GTPase RabG3b functions in autophagy and contributes to tracheary element differentiation in *Arabidopsis*. *The Plant Journal* **64**: 151–164.

Lacayo CI, Malkin AJ, Holman HY, *et al.* 2010. Imaging cell wall architecture in single *Zinnia elegans* tracheary elements. *Plant Physiology* **154**: 121–133.

Li F, Vierstra RD. 2012. Autophagy: a multifaceted intracellular system for bulk and selective recycling. *Trends in Plant Science* **17**: 526–537.

Liu L, Eriksson KEL, Dean JFD. 1999. Localization of hydrogen peroxide production in *Zinnia elegans* L. stems. *Phytochemistry* **52**: 545–554.

Liu Y, Bassham DC. 2012. Autophagy: pathways for self-eating in plant cells. *Annual Review of Plant Biology* **63**: 215–237.

Love MI, Huber W, Anders S. 2014. Moderated estimation of fold change and dispersion for RNA-seq data with DESeq2. *Genome Biology* **15**: 550.

Mao X, Cai T, Olyarchuk JG, Wei L. 2005. Automated genome annotation and pathway identification using the KEGG Orthology (KO) as a controlled vocabulary. *Bioinformatics* **21**: 3787–3793.

Matile P, Winkenbach F. 1971. Function of lysosomes and lysosomal enzymes in senescing corolla of morning glory (*Ipomoea purpurea*). *Journal of Experimental Botany* **22**: 759.

Minami A, Fukuda H. 1995. Transient and specific expression of a cysteine endopeptidase associated with autolysis during differentiation of *Zinnia* mesophyll cells into tracheary elements. *Plant & Cell Physiology* **36**: 1599–1606.

Mitsuda N, Seki M, Shinozaki K, Ohme-Takagi M. 2005. The NAC transcription factors NST1 and NST2 of *Arabidopsis* regulate secondary wall thickenings and are required for anther dehiscence. *The Plant Cell* **17**: 2993–3006.

Nakaune S, Yamada K, Kondo M, *et al.* 2005. A vacuolar processing enzyme, deltaVPE, is involved in seed coat formation at the early stage of seed development. *The Plant Cell* **17**: 876–887.

Novo-Uzal E, Fernández-Pérez F, Herrero J, *et al.* 2013. From *Zinnia* to *Arabidopsis*: approaching the involvement of peroxidases in lignification. *Journal of Experimental Botany* **64**: 3499–3518.

Obara K, Kuriyama H, Fukuda H. 2001. Direct evidence of active and rapid nuclear degradation triggered by vacuole rupture during programmed cell death in *Zinnia*. *Plant Physiology* **125**: 615–626.

Oda Y, Mimura T, Hasezawa S. 2005. Regulation of secondary cell wall development by cortical microtubules during tracheary element differentiation in *Arabidopsis* cell suspensions. *Plant Physiology* **137**: 1027–1036.

Ohashi-Ito K, Oda Y, Fukuda H. 2010. Arabidopsis VASCULAR-RELATED NAC-DOMAIN6 directly regulates the genes that govern programmed cell death and secondary wall formation during xylem differentiation. *The Plant Cell* **22**: 3461–3473.

Paredez AR, Somerville CR, Ehrhardt DW. 2006. Visualization of cellulose synthase demonstrates functional association with microtubules. *Science* **312**: 1491–1495.

Pedroso-de-Moraes C, de Souza-Leal T, Brescansin RL, Pettini-Benelli A, Sajo MdG. 2012. Radicular anatomy of twelve representatives of the Catasetinae subtribe (Orchidaceae: Cymbidieae). *Anais da Academia Brasileira de Ciencias* **84**: 455–467.

Pesquet E, Tuominen H. 2011. Ethylene stimulates tracheary element differentiation in *Zinnia elegans* cell cultures. *New Phytologist* **190**: 138–149.

Pesquet E, Zhang B, Gorzsás A, *et al.* 2013. Non-cell-autonomous postmortem lignification of tracheary elements in *Zinnia elegans*. *The Plant Cell* **25**: 1314–1328.

Porembski S, Barthlott W. 1988. Velamen radicum micromorphology and classification of Orchidaceae. *Nordic Journal of Botany* **8**: 117–137.

Pridgeon AM. 1987. *Orchid biology: reviews and perspectives*. New York: Cornell University Press.

Rogers HJ. 2005. Cell death and organ development in plants. *Current Topics in Developmental Biology* **71**: 225–261.

Rogers HJ. 2006. Programmed cell death in floral organs: how and why do flowers die? *Annals of Botany* **97**: 309–315.

Rojo E, Martin R, Carter C, *et al.* 2004. VPE gamma exhibits a caspase-like activity that contributes to defense against pathogens. *Current Biology* **14**: 1897–1906.

Růžička K, Ursache R, Hejátko J, Helariutta Y. 2015. Xylem development – from the cradle to the grave. *New Phytologist* **207**: 519–535.

Stewart JJ, Akiyama T, Chapple C, Ralph J, Mansfield SD. 2009. The effects on lignin structure of overexpression of ferulate 5-hydroxylase in hybrid poplar. *Plant Physiology* **150**: 621–635.

Suarez MF, Filonova LH, Smertenko A, *et al.* 2004. Metacaspase-dependent programmed cell death is essential for plant embryogenesis. *Current Biology* **14**: R339–R340.

Taylor NG, Laurie S, Turner SR. 2000. Multiple cellulose synthase catalytic subunits are required for cellulose synthesis in *Arabidopsis*. *The Plant Cell* **12**: 2529–2540.

Thelen MP, Northcote DH. 1989. Identification and purification of a nuclease from *Zinnia elegans* L.: a potential molecular marker for xylogenesis. *Planta* **179**: 181–195.

Tokunaga N, Uchimura N, Sato Y. 2006. Involvement of gibberellin in tracheary element differentiation and lignification in *Zinnia elegans* xylogenic culture. *Protoplasma* **228**: 179–187.

Vogt T. 2010. Phenylpropanoid biosynthesis. *Molecular Plant* **3**: 2–20.

Wang KL, Li H, Ecker JR. 2002. Ethylene biosynthesis and signaling networks. *The Plant Cell* **14 Suppl**: S131–S151.

Wightman R, Turner SR. 2008. The roles of the cytoskeleton during cellulose deposition at the secondary cell wall. *The Plant Journal* **54**: 794–805.

Woffenden BJ, Freeman TB, Beers EP. 1998. Proteasome inhibitors prevent tracheary element differentiation in *Zinnia* mesophyll cell cultures. *Plant Physiology* **118**: 419–430.

Yamamoto R, Demura T, Fukuda H. 1997. Brassinosteroids induce entry into the final stage of tracheary element differentiation in cultured *Zinnia* cells. *Plant & Cell Physiology* **38**: 980–983.

Yamamoto R, Fujioka S, Demura T, Takatsuto S, Yoshida S, Fukuda H. 2001. Brassinosteroid levels increase drastically prior to morphogenesis of tracheary elements. *Plant Physiology* **125**: 556–563.

Ye ZH, Droste DL. 1996. Isolation and characterization of cDNAs encoding xylogenesis-associated and wounding-induced ribonucleases in *Zinnia elegans*. *Plant Molecular Biology* **30**: 697–709.

Zhao C, Johnson BJ, Kositsup B, Beers EP. 2000. Exploiting secondary growth in Arabidopsis. Construction of xylem and bark cDNA libraries and cloning of three xylem endopeptidases. *Plant Physiology* **123**: 1185–1196.

Zhong R, Demura T, Ye ZH. 2006. SND1, a NAC domain transcription factor, is a key regulator of secondary wall synthesis in fibers of *Arabidopsis*. *The Plant Cell* **18**: 3158–3170.

Zhong R, Richardson EA, Ye ZH. 2007. The MYB46 transcription factor is a direct target of SND1 and regulates secondary wall biosynthesis in *Arabidopsis*. *The Plant Cell* **19**: 2776–2792.

Zhong R, Lee C, Zhou J, McCarthy RL, Ye ZH. 2008. A battery of transcription factors involved in the regulation of secondary cell wall biosynthesis in *Arabidopsis*. *The Plant Cell* **20**: 2763–2782.

Zhou J, Lee C, Zhong R, Ye ZH. 2009. MYB58 and MYB63 are transcriptional activators of the lignin biosynthetic pathway during secondary cell wall formation in *Arabidopsis*. *The Plant Cell* **21**: 248–266.

Zotz G, Schickenberg N, Albach D. 2017. The velamen radicum is common among terrestrial monocotyledons. *Annals of Botany* **120**: 625–632.

Zotz G, Winkler U. 2013. Aerial roots of epiphytic orchids: the velamen radicum and its role in water and nutrient uptake. *Oecologia* **171**: 733–741.